THE JOURNAL OF PHYSICAL CHEMISTRY C
A JOURNAL OF THE AMERICAN CHEMICAL SOCIETY

pubs.acs.org/JPCC

Article

Electric Potential Distribution Inside the Electrolyte during High Voltage Electrolysis

Lukas Forschner, Evelyn Artmann, Timo Jacob,* and Albert K. Engstfeld*

Cite This: https://doi.org/10.1021/acs.jpcc.2c07873

Read Online

ACCESS | Metrics & More | Article Recommendations | Supporting Information

ABSTRACT: Applying an external potential difference between two electrodes leads to a voltage drop in an ion conducting electrolyte. This drop is particularly large in poorly conducting electrolytes and for high currents. Measuring the electrolyte potential is relevant in electrochemistry, e.g., bipolar electrochemistry, ohmic microscopy, or contact glow discharge electrolysis. Here, we study the course of the electrolyte potential during high voltage electrolysis in an electrolysis cell using two reversible hydrogen electrodes as reference electrodes, placed at different positions in the electrolyte. The electrolysis is performed with a Pt working and stainless steel counter electrode in a KOH solution. A computational COMSOL model is devised which supports the experimentally obtained potential distribution. The influence of the cell geometry on the electrolyte potentials is evaluated. Applying the knowledge of the potential distribution to the formation of a Au oxide surface structure produced during high voltage electrolysis, we find that the amount of oxide formed is related to the current rather than the applied voltage.

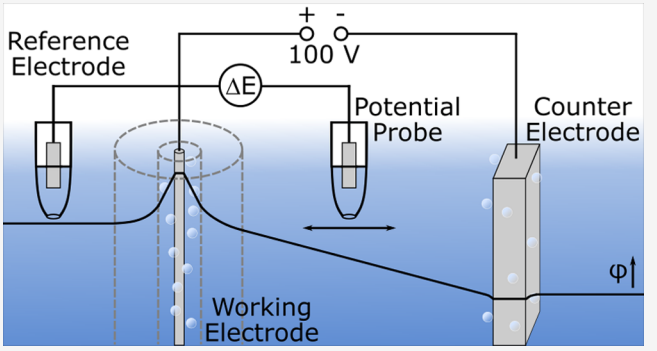

INTRODUCTION

Applying a voltage between two electrodes in an ion conducting electrolyte inevitably leads to a voltage drop between these electrodes. This drop consists of an ohmic drop in the electrolyte which is reciprocally proportional to the electrolyte conductivity. In addition, interfacial voltage drops at the electrode surfaces have to be taken into account. While absolute potentials are not accessible, potential differences between electrodes, as well as between different positions in the electrolyte, can be measured, e.g., by means of reference electrodes.[1−3] Additionally, theoretical simulations can provide insights on the distribution of the electric (electrostatic) potential in the electrolyte.[4−6]

Understanding voltage drops plays an important role in numerous research areas. In classical electrochemical experiments with a three electrode configuration,[7,8] ohmic voltage drops are undesired and need to be compensated for.[9] In bipolar electrochemistry, the voltage drops in a solution can be used to drive reactions on both ends of a conducting electrode placed without electrical connection inside the electrolyte between two driving electrodes.[4,10−13] In ohmic microscopy, two micro reference electrodes probe the voltage drop close to an electrode surface, from which local electrode processes and structures can be inferred.[1,14,15]

There exist several works discussing the cause, consequences, and usability of the voltage drop in the aforementioned examples. This is different for high voltage electrolysis, where high voltages are applied at gas evolving electrodes in the range of a few to several hundred volts.[16] Among other effects, at these voltages, bubble formation becomes significant, which reduces the electrolyte volume around the electrode and hence increases the resistance in that region.[17,18] At very high voltages, even a gas sheath can surround the electrode, in which a plasma can be ignited. This phenomenon is denoted as contact glow discharge electrolysis (CGDE).[16,19−21] Specifically, under these conditions, experimental studies addressing the evolution of the voltage drop around the electrodes and in the electrolyte are scarce. First attempts to consider voltage drops during CGDE were made by Kellogg in 1950, who estimated the voltage drop across the plasma layer by comparing the voltage applied between the driving electrodes to the voltage applied to the electrodes for which the same current is obtained in the nonplasma voltage region.[19] Much later, Slovetskii and Terent'ev measured the potential distribution inside the plasma layer using a movable potential probe.[22] Both studies omit considerations regarding the electrode geometry as well as the electrolyte potential distribution, which were shown to play a major role in other

Received: November 12, 2022
Revised: February 3, 2023

research areas mentioned above.[23−26] In contrast, the potential distribution in an electrolyte (with a given conductivity) close to the electrode under nonplasma conditions (independent of the electrode material) was addressed by Hickling and Ingram in 1963.[20] The authors estimated the voltage drop around a wire electrode based on idealized geometric considerations reported by Kasper[27] to calculate the Joule heating power. Overall, a better understanding of the voltage drop is desirable in high voltage electrolysis, especially in the voltage range where CGDE is observed, in order to understand the underlying physicochemical properties and processes.

The aim of this work is to disentangle voltage drops caused by different effects across the electrolyte during "normal" high voltage electrolysis, i.e., before the onset of CGDE. The electrolysis experiments were performed in 0.01 M KOH using reversible hydrogen reference electrodes (RHEs)[28] to probe the potential distribution in the electrolyte as well as the potentials of the stainless steel counter electrode and the significantly smaller Pt wire anode. All electrolysis experiments in this work were performed in a rectangular glass cell. This setup allows for a flexible and reproducible positioning of the electrodes. Furthermore, the defined geometry of the cell allows for a simple comparison of the measured electric field between the driving electrodes with a computational COMSOL model. Using the knowledge from this complementary experimental and theoretical approach, we will show how electrode materials can be selectively modified. Since Pt does not restructure during high voltage electrolysis, we use Au electrodes instead, which were shown to exhibit a voltage dependent Au oxide formation.[29,30] From our experiments, we will demonstrate that the current density is a better descriptor for the amount of Au oxide formed than the applied voltage.

EXPERIMENTAL SECTION

Materials. The Pt and Au wire electrodes (purity at least 99.99%) were purchased from MaTecK and have a diameter of 0.5 mm. Clean and smooth surfaces were obtained by regular annealing of the wires in a propane flame (MTI) for 3 min. The 0.01 M KOH electrolyte solution was prepared from KOH pellets (99.99%, Sigma-Aldrich) and Milli-Q water (18.2 MΩ cm, TOC ≤ 3 ppb). 3D-printed materials were made from chemically resistant PVDF purchased from 3Dogg.

Electrolysis. All electrolysis experiments were performed in the rectangular glass cell shown in Figure 1a). The cell has a length of 20 cm and a width of 5 cm and was filled with 200 mL of an electrolyte solution resulting in an electrolyte height of 2 cm. A 3D-printed lid is placed on top of the cell, which has grooves on either side, allowing for positioning of the 3D-printed electrode holders and hence the electrodes in the electrolyte. A top view of the lid is shown in Figure 1b). The working electrode (WE) wire was immersed such that it touched the bottom of the cell (length: 2 cm, surface area: 0.314 cm^2). For most experiments, Pt was used as WE material due to its stability during anodic high voltage electrolysis.[29] A counter electrode made of stainless steel (2 × 0.4 × 2 cm) was also immersed such that it touched the bottom of the cell, resulting in an electrolyte contact area of 9.6 cm^2. Reversible hydrogen electrodes (RHEs) were used to measure the local electrolyte potentials. One RHE (REF1) was placed at a fixed position and served as a reference potential for all measurements. Another RHE (REF2) was placed at different positions within the electrolyte. At distances closer than 2 cm to either driving electrode, the REF2 had to be positioned in a tilted

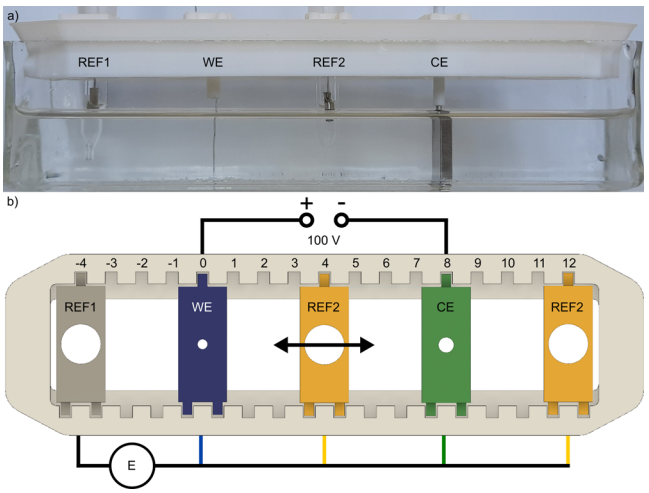

Figure 1. Rectangular electrolysis cell designed for the present work. a) Side view of the cell including the WE, CE, REF1, and REF2. b) Schematic illustration of the electrode holders and their arrangement for the measurement of electrolyte potentials in the first part of this study. The numbers at each electrode position correspond to the distance to the WE center. A voltage of 100 V is applied between the WE (blue) and the CE (green). The potentials at WE, CE, and the reference electrode REF2 (yellow) are measured vs another reference electrode REF1 (gray).

configuration which lowered the positional accuracy. The differences between the potential of REF1 and the potentials at the WE, the CE, and the REF2 were acquired with a National Instruments USB-6009 multifunction DAQ device and an in-house programmed Python software.

To measure high voltages, a voltage divider was placed between the electrodes and the DAQ device, described in more detail in the Supporting Information (Section S1). A constant voltage or a constant current was applied between the WE and the CE using a TDK-Lambda GEN600-1.3 power supply.

Electrochemical Measurements. The electrochemical characterization follows a procedure similar to the one reported in ref 29. Subsequent to the formation of Au oxide on a Au anode during electrolysis as described above, the sample was transferred to another cell to determine the amount of formed Au oxide, which requires clean and defined starting conditions. The cell was a round glass cell (diameter 6 cm) containing 60 mL of 0.01 M KOH. For these kinds of measurements, the shape of the cell does not play a crucial role. Prior to and during each measurement, the electrolyte was deaerated with N_2 to minimize the amount of residual O_2. To determine the amount of Au oxide formed during electrolysis, the Au WE wire was immersed 2 cm in the electrolyte so that the entire oxide but no bare Au was immersed. A Pt sheet (10 × 7.5 mm) served as a CE, and an RHE served as a reference electrode. The potential was controlled with an FHI ELAB potentiostat. Starting from 1.1 V_{RHE}, the WE potential was decreased with a scan rate of 50 mV s^{-1} and held at 0.2 V_{RHE}. During this procedure, first, a large negative (reduction) current was recorded, which decreases with time. When the reduction current was negligible, the surface reduction was thought to be complete. Integrating the total reduction current yields the total charge for reducing the Au oxide, which formed during the electrolysis on the Au electrode. Further potential cycles were recorded between 0.2 and 1.7 V_{RHE} to ensure complete reduction of the oxide.

https://doi.org/10.1021/acs.jpcc.2c07873
J. Phys. Chem. C XXXX, XXX, XXX−XXX

Computational Model. For comparison with the experimentally determined potential distribution in the cell, a computational model was devised with COMSOL Multiphysics 5.6,[31] using the "Electric Currents" interface within the "AC/DC" module. A 2D model reflecting the top view of the cell was designed to accurately reflect its geometry and the electrode positions. Since both the WE and the CE touch the bottom of the cell, horizontal cross sections are identical along the vertical axis; thus, a 2D model is a reasonable approximation of the experimental configuration. The WE and CE materials were set to Pt and steel, respectively. Water was used as an electrolyte, the conductivity of which was set to 2.17 mS cm^{-1}, reflecting the conductivity of a 0.01 M KOH solution at room temperature[32] (see below and SI Section S2). Models with different parameters were used in this work, which is indicated and discussed in the following section.

RESULTS AND DISCUSSION

In the first step, we show the experimentally determined potential distribution in the cell as well as the potentials of the electrolysis electrodes during high voltage electrolysis. For demonstration purposes, 100 V were applied between the Pt wire WE and the CE, separated by 8 cm (see Figure 1), in 0.01 M KOH at room temperature for 5 s. All potentials were measured vs an RHE (REF1) and are shown by the colored markers in Figure 2. The electrolyte potentials were measured

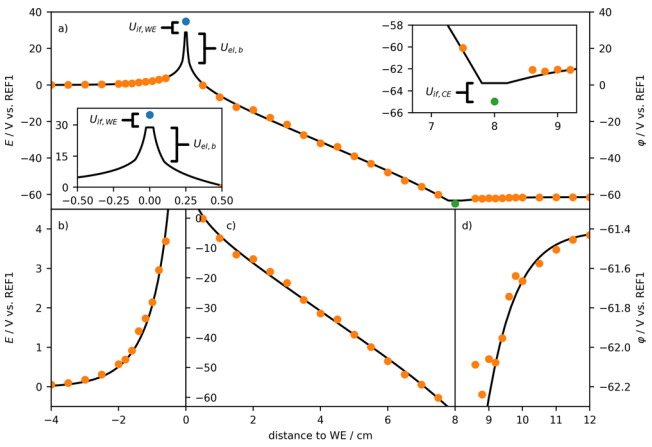

Figure 2. Experimentally obtained potentials inside the electrolyte (orange), at the WE (blue) and the CE (green) as well as the potential distribution obtained from the computational COMSOL model (black, see text for details). All potentials are given vs an RHE at −4 cm (REF1) from the WE. Top row: Overview showing the electrolyte potential in all regions as well as the potentials at the WE and the CE. Bottom row: Magnification of the regions b) close to the WE, c) bulk electrolyte, and d) close to the CE. All potentials were acquired during electrolysis at 100 V between the WE and the CE for 5 s in 0.01 M KOH at room temperature with a Pt wire electrode used as an anode.

using a second RHE (REF2), which was placed at different positions inside the electrolyte, relative to REF1, and are shown in orange. Due to experimental limitations, all positions closer than 2 cm to either electrode have a lower positional accuracy (see the Experimental Section). The potential at the WE (vs REF1) is shown in blue, and that of the CE (vs REF1) is shown in green. Figure 2a) shows the overall potential distribution in the cell. The potential distribution in the electrolyte can be divided into three different regions, shown with higher magnification in Figure 2b) to d). These regions illustrate the potential regions in the electrolyte close to the WE, the bulk electrolyte, and the electrolyte close to the CE. It is apparent that in the electrolyte close to the WE and the CE, the slope of the potential increases the closer REF2 is placed to the respective electrode, while in the electrolyte between the WE and the CE, a more or less linear drop is observed, denoted as the "bulk electrolyte" region.

Focusing on the potential in the bulk electrolyte in Figure 2c), a linear drop of the REF2 potential E with distance x is observed with a slope of $\frac{\Delta E}{\Delta x} = 8.23\ \mathrm{V\ cm^{-1}}$. A linear change is expected when the resistance R in the electrolyte is constant. The electrolyte conductivity can be calculated using the average current of $I = 0.169$ A, the cross-sectional area of the electrolyte in the cell ($A = 10\ \mathrm{cm^2}$), and the potential drop:

$$\Delta E = U = RI = \frac{\Delta x I}{\sigma A} \tag{1}$$

$$\sigma = \frac{I}{A(\Delta E/\Delta x)} \tag{2}$$

From eq 2, the experimentally determined electrolyte conductivity is $\sigma_{exp} = 2.05\ \mathrm{mS\ cm^{-1}}$. This value is similar to that obtained with an empirical formula derived by Gilliam et al. to calculate the conductivity of KOH solutions with different concentrations and temperatures yielding $\sigma_{calc} = 2.39$ mS cm^{-1} (0.01 M KOH and 23.5 °C). Note that the difference between our value and that from the Gilliam equation might be caused by the simplified empirical equation, as discussed in the SI in Section S2.

In the electrolyte region close to the WE in Figure 2b), the electrostatic potential increases more steeply the closer the RHE is placed to the WE. The potential distribution around a symmetrical wire electrode can be calculated using the logarithmic eq 3[20,27] where L is the length of the electrode, and φ_1 and φ_2 are the potentials at the electrode radius r_1 and at a radius r_2 inside the electrolyte, respectively.

$$\varphi_1 - \varphi_2 = \frac{I}{2\sigma\pi L} \ln \frac{r_2}{r_1} \tag{3}$$

The expected evolution of the potential distribution from eq 3 strongly disagrees with our experimental results, which is illustrated and described in the SI (Section S3). The difference is larger at greater distances from the WE. Since the equation was derived for an idealized geometry, we conclude that this simplification is only valid at very small distances and that the cell geometry influences the potential distribution already close to the electrode (< 5 mm).

Similar to the evolution of the potential at the WE, an increasing slope is observed at the CE in Figure 2d), where the potential gets more negative at smaller distances to the CE. The voltage drop is, however, smaller at the CE. This can be explained by the fact that the CE is much larger than the WE, and thus the electrolyte cross-section is larger which in turn results in an overall lower resistance (according to eq 2).

To gain a better understanding of the influence of the cell geometry, a computational COMSOL Multiphysics[31] based model has been devised (see the Experimental Section). The model only considers the electrolyte conduction based on Ohm's law. Aspects such as bubble formation, electrochemical reactions at the electrodes, and changes to local temperature or electrolyte concentration are not considered explicitly.

https://doi.org/10.1021/acs.jpcc.2c07873
J. Phys. Chem. C XXXX, XXX, XXX−XXX

However, it is possible to implicitly treat these processes as we will show below. The temperature effect can be considered to be negligible for our further experimental and theoretical description as the electrolyte temperature increased by at most 0.3 °C during electrolysis (at 100 V for 5 s). A detailed description of the final model is included in the SI in Section S5.

In the first modeling approach, the experimentally measured potentials at the WE and the CE (blue and green points in Figure 2, respectively) were used as electrode potentials. The resulting modeled potential distribution illustrated by the dotted curve in Figure 3 shows qualitatively a good agreement

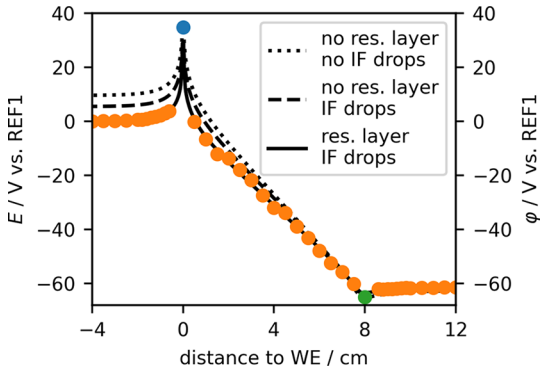

Figure 3. Experimentally obtained potentials at the WE (blue), the CE (green), and inside the electrolyte (orange) as well as potential distributions obtained from computational models (black) including neither interface (IF) drops nor a resistance layer (dotted), including only the IF drops (dashed), and including both IF drops and a layer with increased resistance (solid).

with the experimental results. Nevertheless, small discrepancies remain, which might be caused by bubbles in the electrolyte and the reactions at the electrode.[17,33,34]

In general, the total cell voltage U_{tot} can be expressed as the sum of all voltage drops in the cell according to eq 4. First, we consider that there are voltage drops resulting from the electrolyte resistance close to the WE, $R_{el,WE}$, close to the CE, $R_{el,CE}$, and in the bulk electrolyte, $R_{el,bulk}$. The sum of these resistances gives the total electrolyte resistance R_{el}. Additionally, we expect that there are voltage drops at the electrode | electrolyte interfaces, denoted as $U_{if,WE}$ and $U_{if,CE}$.

$$\begin{aligned} U_{tot} &= U_{el,WE} + U_{el,bulk} + U_{el,CE} + U_{if,WE} + U_{if,CE} \\ &= (R_{el,WE} + R_{el,bulk} + R_{el,CE})\cdot I + U_{if,WE} + U_{if,CE} \\ &= R_{el}\cdot I + U_{if,WE} + U_{if,CE} \end{aligned} \tag{4}$$

To determine the interfacial voltage drops, we recorded polarization curves which are shown in Figure 4a) and the low current−voltage region with higher magnification in Figure 4b). These curves were obtained by applying different constant currents for 5 s between the working electrode and the counter electrode. The total voltage between the WE and the CE, as well as the potentials at the WE and the CE vs RHE1, were measured.

These curves can be rationalized by considering how the total voltage can be divided into the voltage drops at the electrodes and in the electrolyte in eq 4. By measuring the potentials at the WE and the CE, we can separate these contributions further. The WE potential vs REF1 contains the

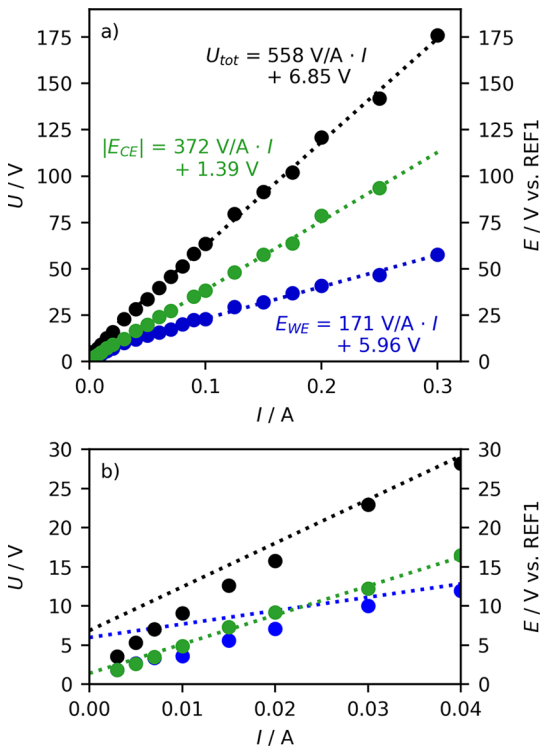

Figure 4. a) Polarization curve recorded with a distance between the WE and the CE of 8 cm in 0.01 M KOH at room temperature. The total voltage between the WE and the CE is shown in black, the WE potential is shown in blue, and the absolute CE potential is shown in green. b) Magnification at low currents.

voltage drop at the WE interface and the electrolyte voltage drop close to the WE according to eq 5.

$$\begin{aligned} E_{WE} &= U_{if,WE} + U_{el,WE} \\ &= U_{if,WE} + R_{el,WE}\cdot I \end{aligned} \tag{5}$$

Similarly, the CE potential contains the voltage drop at the CE interface as well as in the electrolyte close to the CE. Additionally, because the bulk electrolyte is located between the CE and REF1, the bulk electrolyte voltage drop is included, as shown in eq 6.

$$\begin{aligned} -E_{CE} &= U_{if,CE} + U_{el,CE} + U_{el,bulk} \\ |E_{CE}| &= U_{if,CE} + (R_{el,CE} + R_{el,bulk})\cdot I \end{aligned} \tag{6}$$

Eqs 5 and 6 illustrate that both the WE potential and the CE potential contain a part that is proportional to the current, i.e., the voltage drop in the electrolyte. This leads to a linear increase of U_{tot}, E_{WE}, and $|E_{CE}|$ with an increasing current in Figure 4a). The slope of E_{WE} is $R_{el,WE}$, and that of $|E_{CE}|$ is the sum of $R_{el,CE}$ and $R_{el,bulk}$. U_{tot} is proportional to the sum of all these resistances, and thus its slope is the sum of the slopes of $|E_{CE}|$ and E_{WE}.

The voltage drops at the WE and the CE interfaces are, at least for large currents, independent of the current. At small currents, charge transfer resistance dominates, and the current and the overpotential are related in an exponential way, which is described by the Butler−Volmer equation.[35−37] For this reason, U_{tot}, E_{WE}, and $|E_{CE}|$ deviate from the linear relationship at low currents in Figure 4b). Since all other electrolysis experiments in this work were performed at currents larger

https://doi.org/10.1021/acs.jpcc.2c07873
J. Phys. Chem. C XXXX, XXX, XXX−XXX

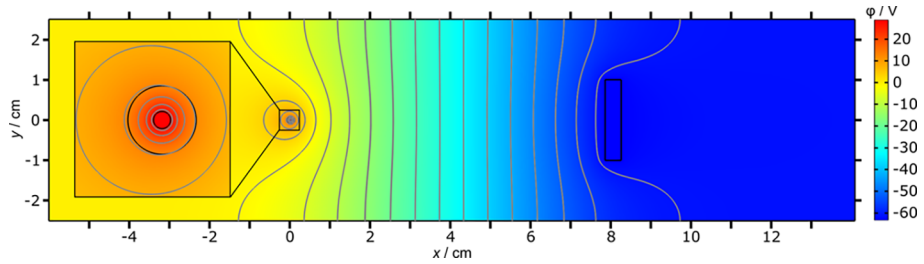

Figure 5. Distribution of the electrolyte potential inferred from the COMSOL model, to simulate the solid curves in Figures 2 and 3. The potential at each position is given by the colors ranging from the WE potential of 28.8 V (red) to the CE potential of −63.3 V (blue). Equipotential lines with distances of 4.6 V are shown in gray. The inset shows a magnification of the area around the WE (smaller black circle) including the layer with increased resistance (between the two black circles).

than 0.1 A, the effect observed in the small-current region has no impact on the further discussion of the results for this work. The current-independent parts of eqs 5 and 6 are the WE and the CE interface drops, respectively. Their values can be extracted from the *y*-axis intersects of the linear region. Thus, the interface voltage drop at the WE is $U_{if,WE}$ = 6.0 V, and that at the CE is $U_{if,CE}$ = 1.4 V. The different magnitudes of these voltage drops can be rationalized as follows. By applying a positive potential at the WE, oxygen will be evolved at the WE, and hydrogen will be evolved at the CE. The equilibrium potential of the latter reaction is 0 V_{RHE} (per definition). The equilibrium potential of the OER is 1.23 V_{RHE}[38,39] and is included in the WE interface drop. In addition, according to the Butler−Volmer formalism, the overpotential depends on the material specific exchange current density and the electrode surface area. Since the CE surface area is much larger than that of the WE, smaller current densities and thus lower overpotentials are needed. Including the experimentally determined interfacial drops at the WE (6.0 V) and the CE (1.4 V) in the COMSOL model results in a potential distribution shown by the dashed line in Figure 3, which matches already quite well with the experimental values.

Finally, we address the possible impact of bubbles in the electrolyte formed in the region around the electrodes during electrolysis on the potential curves. In principle, these bubbles displace the electrolyte close to the electrodes and thus would in fact lead to a smaller electrolyte cross section and hence increase the resistance in this region. This change in conductivity is especially important for the wire WE, since the fraction of the electrolyte displaced by the bubbles is much higher than at the larger CE. To treat the bubbles around the WE implicitly in the COMSOL model, we tentatively added a layer with lower conductivity in the region around the WE. The thickness of the bubble region was arbitrarily chosen as 0.75 mm (measured from the electrode surface). As illustrated in Section S4 in the SI, the thickness of the bubble layer can be varied without affecting the potential distribution in the rest of the cell. In other words, when the width of the bubble layer is increased, the conductivity within that layer also has to be increased, such that the voltage drop in the solution remains unchanged.

To obtain a coherent model, the conductivity within this layer had to be set to $\sigma_{el,b}$ = 1.08 mS cm^{-1}, roughly half that of a bubble free electrolyte, resulting in a voltage drop across the layer with increased resistance of approximately $U_{el,b}$ = 17 V. This decrease in conductivity is, however, quite large, in comparison to the bubbles observed from visual inspection, which do not seem to cover half of the electrode surface or electrolyte volume close to the electrode. Further investigations are required to gain more detailed insights in the volume occupied by bubbles in the solution. Also, other effects can not be ruled out, and therefore, we will tentatively refer to this region as the "layer with increased resistance" without specifying explicitly the reason for this increase.

Including such a layer with increased resistance in the model provides a good match with the experimental values, as shown by the solid lines in Figure 2 and Figure 3. From the model, we derive a current of 0.168 65 A between the WE and CE, which is in good agreement with the average value measured experimentally (0.169 A), demonstrating the validity of the model.

The 2D potential distribution from the model including the layer with increased resistance and the interface voltage drops is shown in Figure 5. The potential is indicated by the colors ranging from 28.8 V (red) at the WE to −63.3 V (blue) at the CE. Additionally, the equipotential lines are shown in gray. In the bulk electrolyte (between x = 2 and 6 cm), the equipotential lines are almost parallel which is in agreement with the linear voltage drop measured experimentally in this region. Very close to the WE, the equipotential lines are almost circular as expected for symmetrical cylinders around a wire electrode.[20,27] However, already at the outer border of the layer with increased resistance (radius 1 mm), a slight distortion of the circular lines is visible (see inset in Figure 5). This distortion is caused by the asymmetry of the cell, which exemplifies that the cell geometry can have a significant influence on the potential distribution, even close to the electrodes. Overall, both the experiment and the model show that the majority of the voltage drops inside the electrolyte according to Ohm's law, and the interface drops $U_{if,We}$ and $U_{if,CE}$ contribute only to a minor degree.

The electrolyte resistance, and thus the voltage drop across the electrolyte, depends on a variety of parameters, such as the cell geometry or the electrolyte composition and temperature. Hence comparison of results, such as $I-U$ curves, obtained in different setups is hardly possible. Thus, applying the same voltage in different setups results in different currents flowing between the WE and the CE. This is of particular importance for electrodes that are modified by (high voltage) electrolysis, and therefore, it is necessary to disentangle the effects of current and voltage.

To illustrate this aspect more clearly, we studied the formation of a Au oxide layer on a Au wire anode during normal electrolysis (see ref 29) as a function of the electrolyte resistance. Note that Au oxide formation is expected to occur at potentials larger than 1.3 V vs RHE.[40] The electrolyte resistance has been varied by a stepwise increase in the distance between the WE and the CE (WE−CE distance) from

https://doi.org/10.1021/acs.jpcc.2c07873
J. Phys. Chem. C XXXX, XXX, XXX−XXX

2 to 8 cm. A constant current of 0.2 A (i.e., a current density of 0.64 A cm^{-2}) or 0.4 A (1.3 A cm^{-2}) has been applied for 30 s. Figure 6a) shows the average voltages between the WE and the

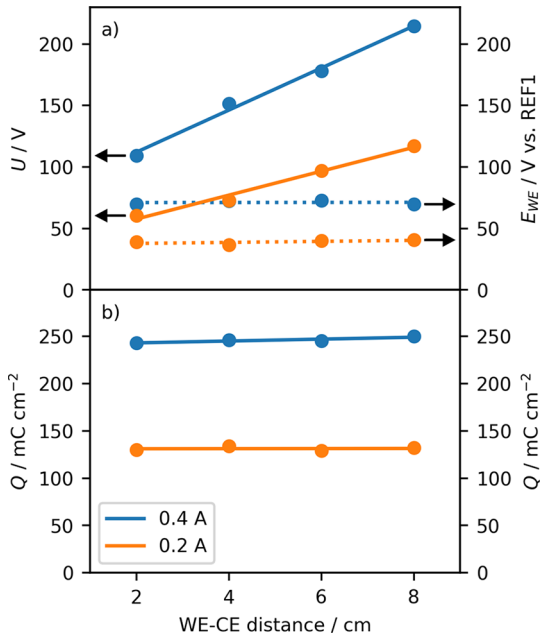

Figure 6. Oxidation of a Au anode during normal electrolysis at 0.2 (orange) and 0.4 A (blue) for 30 s in 0.01 M KOH at room temperature. a) Total voltage between WE and CE (solid lines) as well as WE potentials vs REF1 at −4 cm (dashed lines). b) Amount of charge related to the reduction of Au oxide inferred from electrochemical reduction.

CE, as well as the WE potentials for a certain WE−CE distance and applied current. Each point represents a new measurement with a freshly prepared electrode and electrolyte. As expected, the total voltage increases linearly with electrode distance due to the increase in bulk electrolyte volume in between the electrodes. In contrast, the WE potential remains constant for a given current (density) since the electrolyte around the WE does not change with the electrode distance.

The amount of Au oxide formed during electrolysis can be inferred from the charge passed during the electrochemical reduction of the electrodes (see the Experimental Section and ref 29). The corresponding charges are depicted in Figure 6b). Previous XPS measurements show that primarily Au_2O_3 is formed under these conditions.[30] Hence, the evaluated charge is directly proportional to the amount of Au_2O_3 formed during HV electrolysis.

Applying a current of 0.4 A, roughly twice as much oxide is formed on the Au substrate as when a current of 0.2 A is applied. Nevertheless, for both currents, the amount of surface oxide is independent of the WE−CE distance. The amount of oxide formed at 0.2 and 0.4 A corresponds to around 0.65% of the total charge. The majority of the current results from the OER.

Overall, the fact that the WE potential and the amount of Au oxide do not change for a certain current at different WE−CE distances indicates that the formation of Au oxide only depends on the applied current (or the current density at the WE) rather than on the applied voltage. This is reasonable, since the current density in electrochemistry is related to a reaction rate and thus defines the processes occurring at an electrochemical interface.

CONCLUSION

In this study, we presented a method to determine the potential distribution in an aqueous electrolyte during high voltage electrolysis using reference electrodes. For a cell with a constant cross-sectional area, inside the electrolyte at a certain distance from the driving electrodes, the voltage drops in a linear fashion. In the region around the electrodes, the potential drops more steeply and depends on the distance to the respective electrode. Besides, the drops are larger for the smaller WE compared to the large CE. We suggest that this larger potential drop is caused by the reduced electrolyte cross section by getting closer to the electrode as well as the presence of bubbles located around the electrodes. Note, however, that these phenomena do not yet fully explain the drop in this region, and further investigations are required. Overall, the potential distribution in the electrolyte strongly depends on the cell geometry. Based on our experimental findings, a computational COMSOL model has been devised, yielding a potential distribution that is in good agreement with the experimental values.

The importance of understanding the voltage drop in the solution was illustrated for the Au oxide formation on Au substrates by high voltage electrolysis. By keeping the current constant, but changing the distance between the WE and the CE (increasing the electrolyte resistance), we demonstrated that the oxide formation mainly depends on the current density at the WE. Thus, in order to compare structures formed by HV electrolysis reported in the literature, we encourage the community to report on the current densities passed through the working electrode, which is independent of the cell geometry and electrode positions, rather than reporting the voltage applied between the driving electrodes, which in turn strongly depends on the electrode positions and the cell geometry.

ASSOCIATED CONTENT

Data Availability Statement

The data that support the findings of this study and the COMSOL project are openly available in Zenodo at 10.5281/zenodo.7534249.

Supporting Information

The Supporting Information is available free of charge at https://pubs.acs.org/doi/10.1021/acs.jpcc.2c07873.

Details on voltage divider measurement, comparison of electrolyte conductivity values, comparison of different potential distribution models, variation of thickness of layer with increased resistance, and detailed description of COMSOL model (PDF)

COMSOL report from employed model (PDF)

AUTHOR INFORMATION

Corresponding Authors

Timo Jacob − *Institute of Electrochemistry, Ulm University, D-89081 Ulm, Germany;* orcid.org/0000-0001-7777-2306; Email: timo.jacob@uni-ulm.de

Albert K. Engstfeld − *Institute of Electrochemistry, Ulm University, D-89081 Ulm, Germany;* orcid.org/0000-0002-9686-3948; Phone: +49 (0)731 25401; Email: albert.engstfeld@uni-ulm.de

https://doi.org/10.1021/acs.jpcc.2c07873
J. Phys. Chem. C XXXX, XXX, XXX−XXX

Authors

Lukas Forschner − *Institute of Electrochemistry, Ulm University, D-89081 Ulm, Germany;* orcid.org/0000-0002-1551-5045

Evelyn Artmann − *Institute of Electrochemistry, Ulm University, D-89081 Ulm, Germany;* orcid.org/0000-0003-0789-2841

Complete contact information is available at: https://pubs.acs.org/10.1021/acs.jpcc.2c07873

Author Contributions

L. Forschner: Conceptualization, Formal Analysis, Investigation, Validation, Visualization, Writing - Original Draft Preparation. **E. Artmann**: Writing - Review & Editing. **T. Jacob**: Funding Acquisition, Resources, Supervision, Writing - Review & Editing. **A. K. Engstfeld**: Funding Acquisition, Conceptualization, Supervision, Writing - Review & Editing

Notes

The authors declare no competing financial interest.

■ ACKNOWLEDGMENTS

The authors gratefully acknowledge support by the DFG (German Research Foundation) through the collaborative research center SFB-1316 (project ID: 327886311) as well as the state of Baden-Württemberg and the DFG through grant no. INST 40/574-1 FUGG.

■ REFERENCES

(1) Cartier, C. A.; Kumsa, D.; Feng, Z.; Zhu, H.; Scherson, D. A. Quantitative Aspects of Ohmic Microscopy. *Anal. Chem.* **2012**, *84*, 7080−7084.

(2) Janssen, L. J. J.; Geraets, J. J. M.; Barendrecht, E.; van Stralen, S. D. J. Ohmic Potential Drop During Alkaline Water Electrolysis. *Electrochim. Acta* **1982**, *27*, 1207−1218.

(3) Miller, B.; Bellavance, M. I. Measurement of Current and Potential Distribution at Rotating-Disk Electrodes. *J. Electrochem. Soc.* **1973**, *120*, 42−53.

(4) Li, M.; Liu, S.; Jiang, Y.; Wang, W. Visualizing the Zero-Potential Line of Bipolar Electrodes with Arbitrary Geometry. *Anal. Chem.* **2018**, *90*, 6390−6396.

(5) Fosdick, S. E.; Crooks, J. A.; Chang, B.-Y.; Crooks, R. M. Two-Dimensional Bipolar Electrochemistry. *J. Am. Chem. Soc.* **2010**, *132*, 9226−9227.

(6) Zhou, Y.; Shida, N.; Koizumi, Y.; Watanabe, T.; Nishiyama, H.; Tomita, I.; Inagi, S. Template-free Perpendicular Growth of a Poly(3,4-ethylenedioxythiophene) Fiber Array by Bipolar Electrolysis under an Iterative Potential Application. *J. Mater. Chem. C* **2019**, *7*, 14745−14751.

(7) Hickling, A. Studies in Electrode Polarization. Part IV.-The Automatic Control of the Potenital of a Working Electrode. *Trans. Faraday Soc.* **1942**, *38*, 27−33.

(8) Colburn, A. W.; Levey, K. J.; O'Hare, D.; Macpherson, J. V. Lifting the Lid on the Potentiostat: a Beginner's Guide to Understanding Electrochemical Circuitry and Practical Operation. *Phys. Chem. Chem. Phys.* **2021**, *23*, 8100−8117.

(9) Oelßner, W.; Berthold, F.; Guth, U. The iR Drop - Well-known but often Underestimated in Electrochemical Polarization Measurements and Corrosion Testing. *Mater. Corros.* **2006**, *57*, 455−466.

(10) Fosdick, S. E.; Knust, K. N.; Scida, K.; Crooks, R. M. Bipolar Electrochemistry. *Angew. Chem., Int. Ed.* **2013**, *52*, 10438−10456.

(11) Shida, N.; Zhou, Y.; Inagi, S. Bipolar Electrochemistry: A Powerful Tool for Electrifying Functional Material Synthesis. *Acc. Chem. Res.* **2019**, *52*, 2598−2608.

(12) Loget, G.; Zigah, D.; Bouffier, L.; Sojic, N.; Kuhn, A. Bipolar Electrochemistry: From Materials Science to Motion and Beyond. *Acc. Chem. Res.* **2013**, *46*, 2513−2523.

(13) Rahn, K. L.; Anand, R. K. Recent Advancements in Bipolar Electrochemical Methods of Analysis. *Anal. Chem.* **2021**, *93*, 103−123.

(14) Chen, Y.; Belianov, A.; Scherson, D. Spatially-Resolved Interfacial Electrochemistry: Ohmic Microscopy. *J. Phys. Chem. C* **2008**, *112*, 8754−8758.

(15) Feng, Z.; Georgescu, S.; Scherson, D. A. New Advances in Ohmic Microscopy. *Russ. J. Electrochem.* **2017**, *53*, 1003−1010.

(16) Yerokhin, A.; Mukaeva, V. R.; Parfenov, E. V.; Laugel, N.; Matthews, A. Charge Transfer Mechanisms Underlying Contact Glow Discharge Electrolysis. *Electrochim. Acta* **2019**, *312*, 441−456.

(17) Vogt, H.; Thonstad, J. The Diversity and Causes of Current-Potential Behaviour at Gas-Evolving Electrodes. *Electrochim. Acta* **2017**, *250*, 393−398.

(18) Wüthrich, R.; Comninellis, C.; Bleuler, H. Bubble Evolution on Vertical Electrodes under Extreme Current Densities. *Electrochim. Acta* **2005**, *50*, 5242−5246.

(19) Kellogg, H. H. Anode Effect in Aqueos Electrolysis. *J. Electrochem. Soc.* **1950**, *97*, 133−142.

(20) Hickling, A.; Ingram, M. D. Contact Glow-Discharge Electrolysis. *Trans. Faraday Soc.* **1964**, *60*, 783−793.

(21) Sengupta, S. K.; Singh, R. Cathodic Contact Glow Discharge Electrolysis: its Origin and Non-Faradaic Chemical Effects. *Plasma Sources Sci. Technol.* **2017**, *26*, 015005.

(22) Slovetskii, D. I.; Terent'ev, S. D. Parameters of an Electric Discharge in Electrolytes and Physicochemical Processes in an Electrolyte Plasma. *High Energy Chem.* **2003**, *37*, 310−316.

(23) Newman, J. Resistance for Flow of Current to a Disk. *J. Electrochem. Soc.* **1966**, *113*, 501−502.

(24) Cahan, B.; Nagy, Z.; Genshaw, M. A. Cell Design for Potentiostatic Measuring System. *J. Electrochem. Soc.* **1972**, *119*, 64−69.

(25) Hong, S. H.; Kraiya, C.; Lehmann, M. W.; Evans, D. H. Evaluation of Uncompensated Solution Resistance for Electrodes with Spherical-Cap Geometry. *Anal. Chem.* **2000**, *72*, 454−458.

(26) Myland, J. C.; Oldham, K. B. Uncompensated Resistance. 1. The Effect of Cell Geometry. *Anal. Chem.* **2000**, *72*, 3972−3980.

(27) Kasper, C. The Theory of the Potential and the Technical Practice of Electrodeposition: I. The General Problem and the Cases of Uniform Flow. *Trans. Electrochem. Soc.* **1940**, *77*, 353−363.

(28) Jerkiewicz, G. Standard and Reversible Hydrogen Eelctrodes: Theory, Design, Operation, and Applications. *ACS Catal.* **2020**, *10*, 8409−8417.

(29) Artmann, E.; Menezes, P. V.; Forschner, L.; Elnagar, M. M.; Kibler, L. A.; Jacob, T.; Engstfeld, A. K. Structural Evolution of Pt, Au and Cu Anodes by Electrolysis up to Contact Glow Discharge Electrolysis in Alkaline Electrolytes. *ChemPhysChem* **2021**, *22*, 2429−2441.

(30) Artmann, E.; Forschner, L.; Schüttler, K.; Al-Shakran, M.; Jacob, T.; Engstfeld, A. K. Nanoporous Au Formation on Au Substrates via High Voltage Electrolysis. *ChemPhysChem* **2022**, DOI: 10.1002/cphc.202200645.

(31) COMSOL AB, *COMSOL Multiphysics*; Stockholm, Sweden. www.comsol.com (accessed 2023-01-13).

(32) Gilliam, R. J.; Graydon, J. W.; Kirk, D. W.; Thorpe, S. J. Review of Specific Conductivities of Potassium Hydroxide Solutions for Various Concentrations and Temperatures. *Int. J. Hydrog. Energy* **2007**, *32*, 359−364.

(33) Vogt, H.; Balzer, R. The Bubble Coverage of Gas-evolving Electrodes in Stagnant Electrolytes. *Electrochim. Acta* **2005**, *50*, 2073−2079.

(34) Vogt, H. The Actual Current Density of Gas-evolving Electrodes - Notes on the Bubble Coverage. *Electrochim. Acta* **2012**, *78*, 183−187.

(35) Erdey-Grúz, T.; Volmer, M. Zur Theorie der Wasserstoffüberspannung. *Z. Phys. Chem.* **1930**, *150A*, 203.

(36) Butler, J. A. V. The Mechanism of Overvoltage and its Relation to the Combination of Hydrogen Atoms at Metal Electrodes. *Trans. Faraday Soc.* **1932**, *28*, 379−382.

(37) Dickinson, E. J. F.; Wain, A. J. The Butler-Volmer Equation in Electrochemical Theory: Origins, Value, and Practical Application. *J. Electroanal. Chem.* **2020**, *872*, 114145.
(38) Zeng, K.; Zhang, D. Recent Progress in Alkaline Water Electrolysis for Hydrogen Production and Applications. *Prog. Energy Combust. Sci.* **2010**, *36*, 307−326.
(39) Amores, E.; Rodríguez, J.; Oviedo, J.; de Lucas-Consuegra, A. Development of an operation strategy for hydrogen production using solar PV energy based on fluid dynamic aspects. *Open Engineering* **2017**, *7*, 141−152.
(40) Tremiliosi-Filho, G.; Antonia, L. D.; Jerkiewicz, G. Limit to Extent of Formation of the Quasi-two-dimensional Oxide State on Au Electrodes. *J. Electroanal. Chem.* **1997**, *422*, 149−159.

https://doi.org/10.1021/acs.jpcc.2c07873
J. Phys. Chem. C XXXX, XXX, XXX−XXX